Digest Journal of Nanomaterials and Biostructures Vol. 19, No. 4, October-December 2024, p. 1737-1755

# Photocatalytic performance of Ag/$CuBi_2O_4$/$TiO_2$ heterostructures

M. H. Huang [a], K. C. Hsu [b], T. H. Fang [a,c,*], C. J. Shih [c], Y. S. Fu [d]

[a] *Department of Mechanical Engineering, National Kaohsiung University of Science and Technology, Kaohsiung 80778, Taiwan*

[b] *Department of Marine Engineering, National Kaohsiung University of Science and Technology, Kaohsiung 80543, Taiwan*

[c] *Department of Fragrance and Cosmetic Science, College of Pharmacy, Kaohsiung Medical University, Kaohsiung 80708, Taiwan*

[d] *Department of Greenergy, National University of Tainan, Tainan 701027, Taiwan*

In this study, $CuBi_2O_4$ materials were synthesized using a solid-state reaction method. $CuBi_2O_4$ and $TiO_2$ materials were mixed in different proportions. After verifying that $CuBi_2O_4$ and $TiO_2$ are in a 1:5 ratio, optimal photodegradation of methylene blue under UV light irradiation is achieved. Under the existing heterostructure nanocatalyst of $CuBi_2O_4$ and $TiO_2$, when a little noble metal or rare earth element is doped, a little Ag is added to understand the changes in photocatalysis and its characteristics. The Ag-doped $TiO_2$ powder was ground with the optimal quantitative ratio of $CuBi_2O_4$ powder to form Ag/$TiO_2$/$CuBi_2O_4$ heterostructure catalysts for photocatalytic degradation evaluation. Photocatalytic behavior in methylene blue degradation under UV-light irradiation demonstrates that the Ag/$TiO_2$/$CuBi_2O_4$ heterostructure nanocatalyst, doped with 11 wt.% Ag, achieves superior photocatalytic activity. The degradation efficiency reaches 82.65% after 2 hours, which is a significant improvement of 34.28% over the original $CuBi_2O_4$/$TiO_2$'s 48.37%. Finally, the photocatalytic mechanism of $CuBi_2O_4$/$TiO_2$ in Ag-doped heterostructure nanocatalysts was discussed.

(Received September 3, 2024; Accepted November 12, 2024)

*Keywords:* The solid-state reaction method, Photodegradation, Heterostructure, Nanocatalyst, Photocatalysis, Nanocomposite, Methylene blue, Mechanism

* Corresponding author: fang.tehua@msa.hinet.net

https://doi.org/10.15251/DJNB.2024.194.1737

## 1. Introduction

Clean water resources have always been a necessary element for human survival. With the development of industrial technology, harmful substances have also polluted the environment, particularly through wastewater pollution [1]. Generally, an effective treatment method for organic wastewater is to use organic semiconductor materials for photocatalytic degradation [2-6]. Semiconductor materials often used in photocatalysis include $TiO_2$, ZnO, $WO_3$, $SnO_2$, $SiO_2$, $Bi_2O_3$, $Fe_2O_3$ and $BiFeO_3$ [7-27]. Among them, $TiO_2$ has the best photocatalytic effect, so $TiO_2$ is frequently used in photocatalysis [28, 29]. $TiO_2$, an n-type semiconductor, exists in three distinct crystal structures: anatase, rutile, and brookite. However, only the anatase structure has optical properties and catalytic performance among these three crystal structures [25, 26]. Anatase-structured $TiO_2$ features high oxidation energy, robust chemical stability, and is non-toxic [30]. At present, it stands out as one of the most promising photocatalytic materials. Given that the energy gap of anatase $TiO_2$ is approximately 3.2 eV, it requires excitation of electrons from the valence band to the conduction band. [7], the irradiation range of the photocatalytic active reaction is the ultraviolet region [7, 28, 31], and in the photocatalytic efficiency capability under solar visible light is only about 3~5% [28, 32]. Therefore, it has excellent photocatalytic efficiency capability when used in ultraviolet light irradiation for photocatalytic reactions [33].

It is widely recognized that utilizing wide-bandgap and narrow-bandgap semiconductors for sensitization is an effective strategy to enhance the photocatalytic efficiency of these catalysts [34, 35]. Compared with single semiconductors, composite photocatalysts have multiple advantages under ultraviolet-visible light irradiation. First, light trapping can be significantly improved through the simultaneous excitation of coupling materials [34]. According to some study reporters, wide and narrow bandgap semiconductors with energy band potential often combine semiconductor materials to improve the segregation of photoexcited electrons and holes while efficiently inhibiting and preventing their recombination. Matching of combined heterojunction interfaces [25].

$CuBi_2O_4$ is a typical p-type semiconductor photocatalytic material [36], with a narrow energy gap band of 1.5-1.8 eV [36-38]; compared to the energy gap of n-type $TiO_2$ of about 3.2 eV, $CuBi_2O_4$ and $TiO_2$ are in the p-n heterojunction is a matched semiconductor material photocatalyst. The heterojunction formation is a significant advantage of carrier transport at the interface [36]. Because they each have different energy gap bands, the heterogeneous combination of visible light-absorbing photocatalysts and ultraviolet light-absorbing photocatalysts can obtain a wide light capture range [39], which can effectively improve the charge separation and light absorption of the photocatalysts. The catalytic activity combines photocatalyst heterostructures with high activity and photo responsiveness [39].

In this experiment, the primary purpose is to use the quantitative ratio of p-$CuBi_2O_4$/n-$TiO_2$ heterostructure semiconductor material as the base material. Doping the noble metal Ag element can mainly prevent electrons from recombination through electron transfer and improve photocatalytic

efficiency [2, 40-43]. During the preparation process, a quantitative amount of $TiO_2$ powder was first doped with different weights of Ag and then mixed with a quantitative amount of $CuBi_2O_4$ powder and ground for three hours to study its photocatalytic performance and characteristics under ultraviolet light irradiation. Employ techniques such as EDS (energy dispersive X-ray spectroscopy), SEM (scanning electron microscopy), X-ray diffraction, UV-visible spectroscopy, UV-visible spectrophotometry, and fluorescence spectrophotometry to explore and examine the differences in the $CuBi_2O_4/TiO_2$ doping weight ratio of powder to Ag.

## 2. Materials and methods

In this experiment, the primary photocatalytic materials were the preparation of $CuBi_2O_4$ [28], $TiO_2$ powder (Sigma-Aldrich), obtaining Ag from $AgNO_3$ (Fluka), and using methylene blue solution as the organic pollutant.

$CuBi_2O_4$ powder was prepared using a rapid vibro-milling method. Bismuth oxide powder ($Bi_2O_3$, 99.0%, Alfa Aesar) and copper oxide powder (CuO, 99.0%, Alfa Aesar) were weighed at a ratio of 1:1 After mixing and grinding through a planetary ball mill for three hours, the high-temperature furnace is then subjected to sintering with a controlled heating rate of 5 °C per minute. The sintering temperatures for synthesizing $CuBi_2O_4$ are 600, 650, 700, and 750 °C and maintained for 25 hours.

In the first stage, $CuBi_2O_4$ powder and $TiO_2$ powder are mixed at a weight ratio of (1:10, 2:10, 3:10, and 4:10) respectively, and ground using a planetary ball mill for 3 hours and then mixed with methylene blue for organic contamination. The solution was subjected to photocatalytic experiments to confirm the optimal ratio of $CuBi_2O_4$ and $TiO_2$ under photocatalysis.

In addition, the $CuBi_2O_4/TiO_2$ powder is not doped with Ag element. First, mix the silver nitrate ($AgNO_3$, Fluka) crystal grains and the quantitative titanium dioxide powder ($TiO_2$, Sigma-Aldrich) and add an appropriate amount of deionized water and stir before proceeding. Drying and sintering, to obtain Ag element from $AgNO_3$, sintering is performed for one hour at a temperature exceeding the boiling point of $AgNO_3$ of 440 °C. Finally, quantitative $TiO_2$ was doped with different weights of Ag (0, 1, 3, 5, 7, 9, 11, and 13 wt.%), and a quantitative weight of $CuBi_2O_4$ was mixed and ground with a planetary ball mill for 3 hours.

Finally, $CuBi_2O_4$ powder and $TiO_2$ were doped with Ag element materials of different concentrations as photocatalytic materials and methylene blue organic pollutants for photocatalytic experiments.

In this experiment, the structure of the powder was studied through X-ray diffraction (XRD, Malvern Panalytical Aeris) analysis. The parameters were configured with Cu-Kα rays ($\lambda$ = 1.5406 Å) as the light source, a voltage of 10 kV, a current of 8 A, a scan rate of 0.2°/s, and a scan range spanning from 10° to 80°. The test results were compared with the diffraction peaks from the Joint

Committee on Powder Diffraction Standards (JCPDS) card, and the Scherrer equation (1) was utilized to determine the grain size [2]:

$$D = 0.9\lambda/\beta \cos\theta \quad (1)$$

where $D$ represents the crystallite size, $\beta$ represents the full width at half maximum (FWHM) of th e reflection, $\theta$ represents the Bragg angle, and $\lambda$ represents the wavelength of the X-rays (Cu- Kα, λ = 1.5406 Å) [2].

A scanning electron microscope (SEM, Phenom ProX) was used to observe the surface morphology of the samples and measure their size, length, and thickness. Energy dispersive spectroscopy (EDS) measurements and mapping analysis of elemental components were also performed.

The absorption spectrum and UV-visible spectrophotometer (Jasco, V-670) were used to analyze the absorption intensity and energy gap of the sample. Excitation spectra in the 350 to 500 nm wavelength range were obtained using a photoluminescence (PL) spectrometer (Hitachi, F-7000) with an emission wavelength of 260 nm.

In the photocatalytic activity experiment, two 8-watt UV lamps were used as the light source, and the dye concentration was measured with a UV-visible light spectrum analyzer (Shimadzu, UV-1800, UV spectrophotometer), used to analyze dye concentration and the photodegradation effect. First, prepare 125 mL of 10 ppm methylene blue solution, add 0.1 g of photocatalyst into the dye solution, and then use a magnetic stirrer in a dark environment under 20 °C to achieve equilibrium between adsorption and desorption. The methylene blue solution containing the photocatalyst was then irradiated with UV light, and the solution was withdrawn and centrifuged every 20 minutes. Finally, the dye concentration is measured using a UV-visible spectrophotometer. Degradation rate is calculated as follows [2]:

$$\eta = \frac{C_0 - C}{C_0} \times 100\% \quad (2)$$

where $\eta$ represents the efficiency of degradation, $C_0$ represents the initial concentration, and $C$ represents the concentration after exposure [2].

## 3. Results and discussions

XRD analysis was conducted on four samples at varying temperatures. Fig. 1 illustrates the XRD patterns of $CuBi_2O_4$ synthesized through sintering at different temperatures. In Fig. 2, it is shown that the central 2θ peak diffraction angles of $CuBi_2O_4$ at 700 °C are consistent with the JCPDS

card $CuBi_2O_4$ (42-0334), which indicates that the $CuBi_2O_4$ crystal belongs to the tetragonal geometric structure [44-46], The central peak (211) shows a notable increase in intensity, and the product after $CuBi_2O_4$ sintering is in powder form [28]. The color of the sample changes from dark green at 600 °C to black at 700 °C [28]. Therefore, it was found in the experiment that the optimal reaction temperature for preparing $CuBi_2O_4$ photocatalyst is 700 °C [28]. In addition, calculated through Scherrer equation (1), the grain diameter of $CuBi_2O_4$ is approximately 39.12 nm [28].

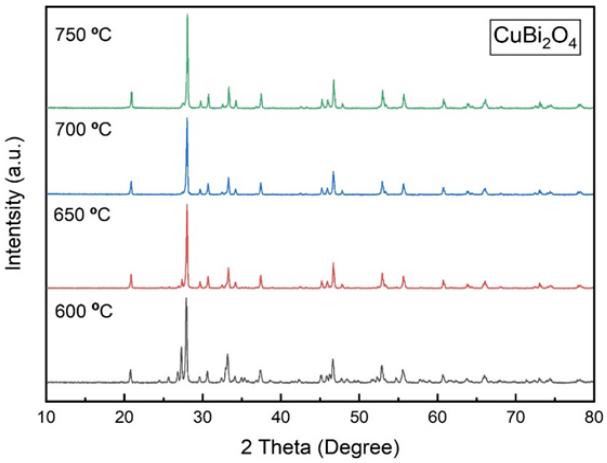


*Fig. 1. X-ray diffraction patterns of $CuBi_2O_4$ samples prepared at different temperatures.*

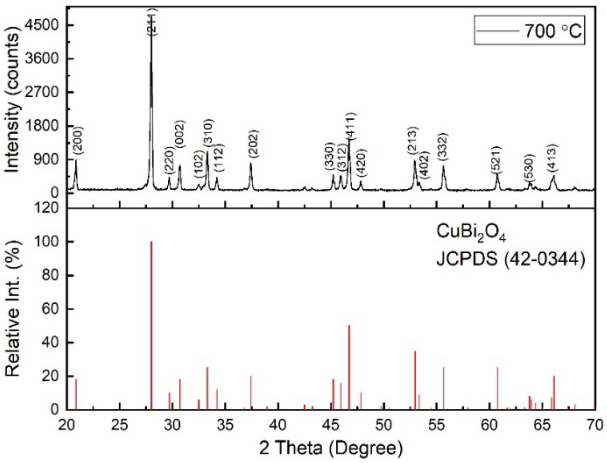


*Fig. 2. X-ray diffraction patterns of prepared samples at 700 °C and the standard data.*

To determine the optimal efficiency of $CuBi_2O_4$ and $TiO_2$ in photodegradation under UV light, the ratios of $CuBi_2O_4/TiO_2$ photocatalytic materials were set to 1:10, 2:10, 3:10, and 4:10, respectively. The powder was added at 0.1 g to 125 ml of solvent dye with methylene blue at a concentration of 10 ppm. Then, samples of the methylene blue solution were taken out every 20

minutes during the experiment, and centrifugation was performed to measure the concentration of methylene blue and observe the photocatalytic degradation of methylene blue during the two-hour photocatalytic experiment. Fig. 3 (a) and (b) respectively illustrate that in different weight ratios of $CuBi_2O_4/TiO_2$, the degradation efficiencies in a solution with a concentration of 10 ppm methylene blue are 45.16%, 48.37%, 39.39%, and 30.44%, respectively changes in photocatalytic degradation concentration per hour. The results show that the $CuBi_2O_4/TiO_2$ ratio configuration of 2:10 is in the heterostructure material with 10 g of $TiO_2$ added with 20 wt.% $CuBi_2O_4$, the maximum photocatalytic activity is 48.37%.

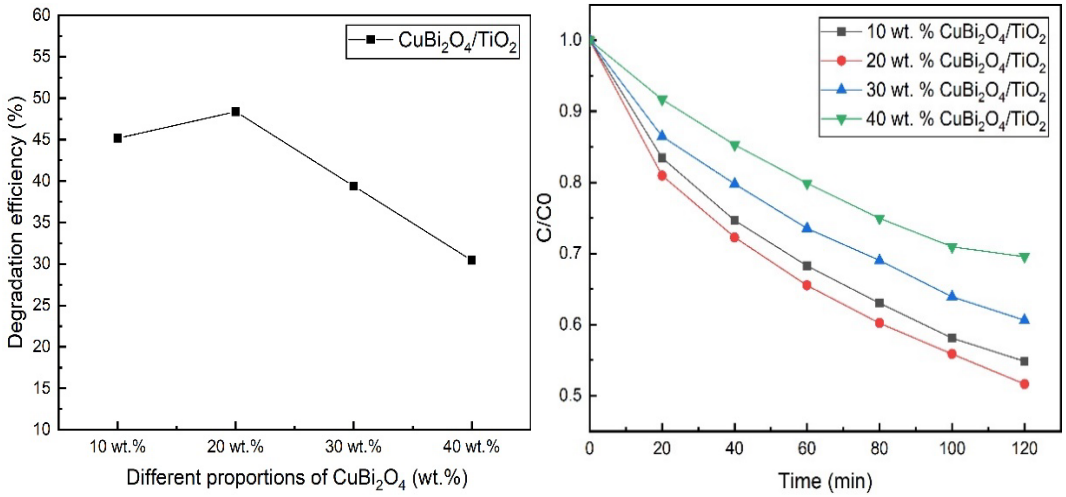


*Fig. 3. (a) Effect of $TiO_2$ and different proportions of $CuBi_2O_4$ on the photocatalytic performance of MB and (b) the concentration changes of MB solution in two hours in the presence of $CuBi_2O_4/TiO_2$ composite materials under UV light irradiation.*

Fig. 4 shows the XRD of $CuBi_2O_4/TiO_2$ and seven sample powders doped with heavy Ag at different concentrations. As the concentration of Ag doping increases, the peak intensity of Ag does not increase significantly; in addition, substitute their peak measured values into Scherrer equation (1) for the calculation and grain sizes were obtained in sequence as 34.17, 35.06, 26.66, 27.97, 26.49, 32.32 and 31.64 nm, respectively. As shown in Fig. 5, the JCPDS Card contrast XRD peaks of $CuBi_2O_4/TiO_2$/11 wt.% Ag and each compound are consistent with the XRD peaks of doped 11 wt.% Ag metal elements.

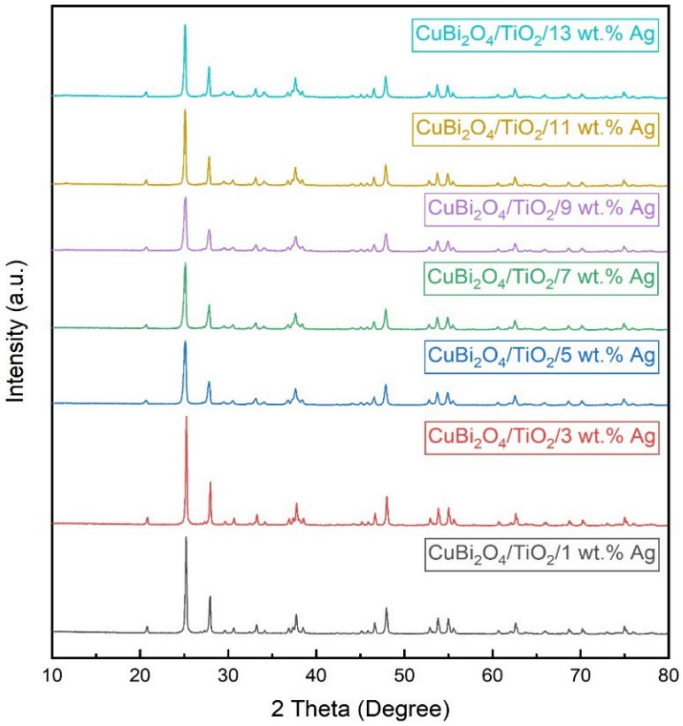


*Fig. 4. X-ray diffraction patterns of $CuBi_2O_4/TiO_2$ composites doped with different proportions of Ag.*

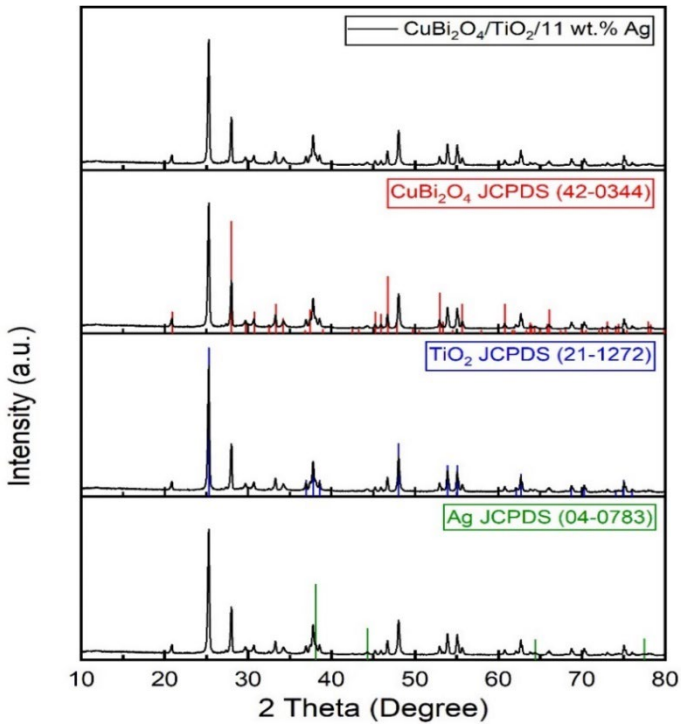


*Fig. 5. X-ray diffraction patterns of $CuBi_2O_4/TiO_2$/11 wt.% Ag composites compared to all JCPDS cards.*

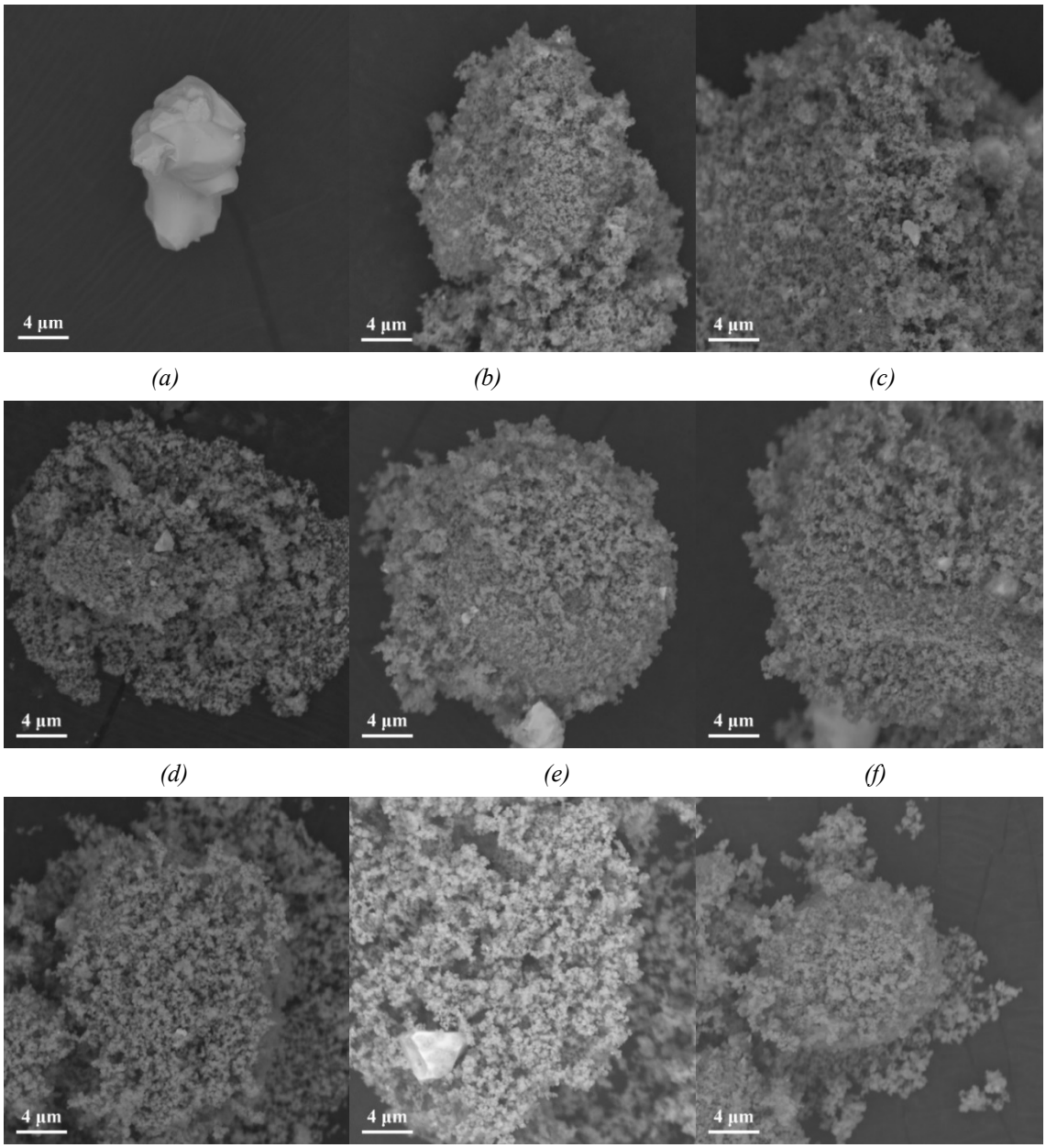


*Fig. 6. SEM images of (a) $CuBi_2O_4$, (b) $CuBi_2O_4/TiO_2$, (c) $CuBi_2O_4/TiO_2$/1 wt.% Ag, (d) $CuBi_2O_4/TiO_2$/3 wt.% Ag, (e) $CuBi_2O_4/TiO_2$/5 wt.% Ag, (f) $CuBi_2O_4/TiO_2$/7 wt.% Ag, (g) $CuBi_2O_4/TiO_2$/9 wt.% Ag, (h) $CuBi_2O_4/TiO_2$/11 wt.% Ag, and (i) $CuBi_2O_4/TiO_2$/13 wt.% Ag.*

In this study, a scanning electron microscope (SEM) was employed to examine the surface morphology of the mixed powder. Fig. 6 (a) is pure $CuBi_2O_4$ and (b)~(i) are SEM images of $CuBi_2O_4/TiO_2$ doped with 1 to 13 wt.% Ag. Fig. 6 (a) shows the sintered morphology of $CuBi_2O_4$ without ball milling, which displays a polyhedral and amorphous shape; Fig. 6(b)~(i) SEM images show the $CuBi_2O_4/TiO_2$ powder doped with different concentrations of heavy Ag, respectively. The eight samples exhibit uniform particle size and consistent morphology, with no discernible changes attributed to the increase in Ag concentration. To judge whether the sample is evenly mixed, in the sample $CuBi_2O_4/TiO_2$/11 wt.% Ag powder, through EDS measurement and mapping detection, and atomic content analysis, the ratio of the number of atoms in the sample and the distribution of the detected atoms can be obtained case. The results are illustrated in Fig. 7 (a) and (c), displaying the

SEM images of the sample along with the corresponding sampling range. Fig. 7 (b) is the EDS analysis chart of each atomic element. In addition, Tab. 1 presents the SEM images for the various nuclear components within the sampling range. The analysis results in the atomic number and weight of each atomic element being close to the proportion of each component. In Fig. 7 (d)~(h), which shows the distribution diagrams of O, Ti, Ag, Bi, and Cu elements, respectively, the atomic number distribution of each element is uniform, and the atomic number of O and Ti elements accounts for the majority. The number of atoms is relatively rare compared to Bi and Cu.

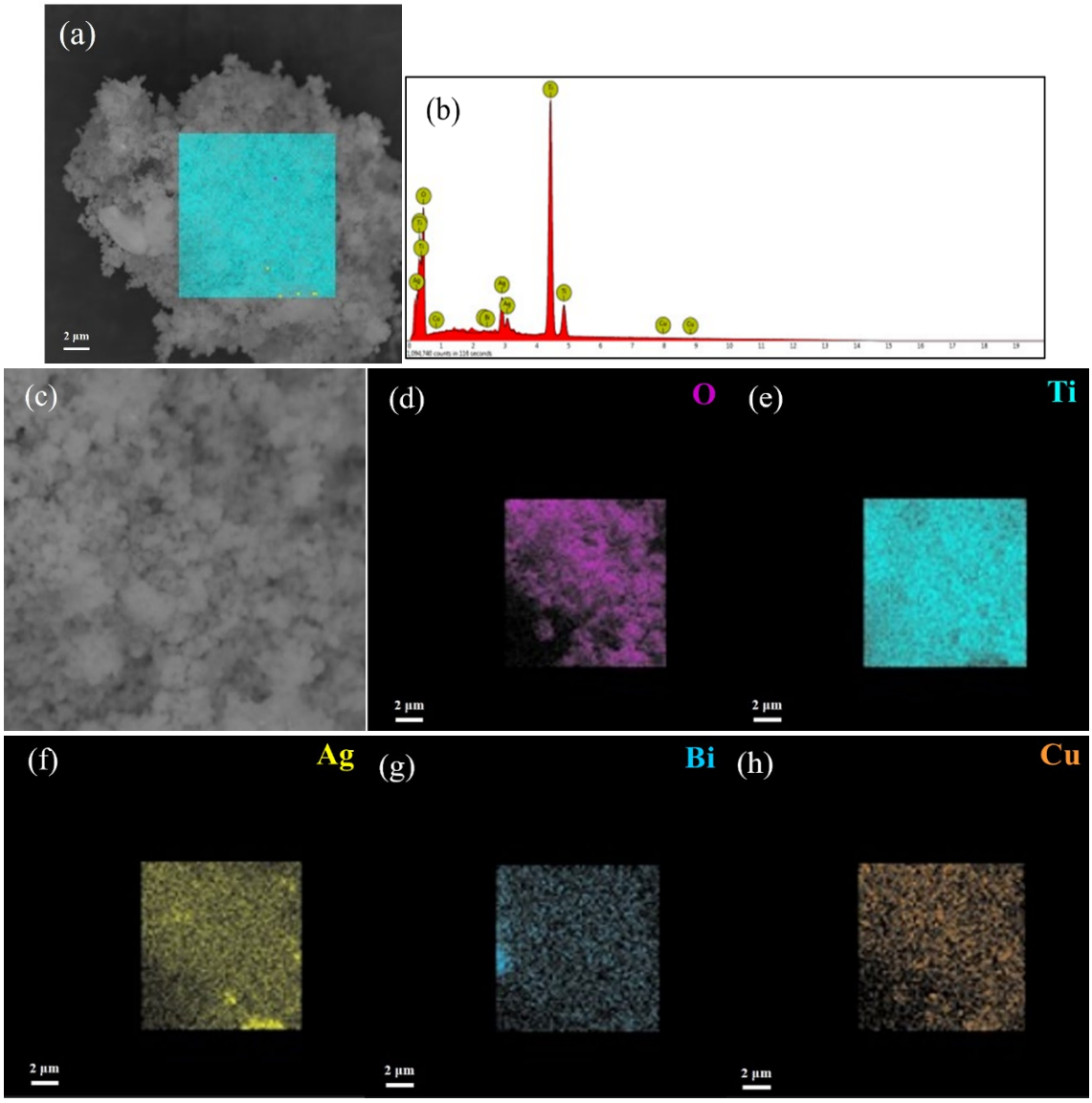


*Fig. 7. The element mapping and EDS analysis, (a) $CuBi_2O_4/TiO_2$/11 wt.% Ag elemental mapping of selected area range, (b) EDS spectra, (c) The selected area imaged, (d) O mapping, (e) Ti mapping, (f) Ag mapping, (g) Bi mapping, and (h) Cu mapping.*

*Table 1. Weight and atomic percentage of the elements in $CuBi_2O_4/TiO_2$/11 wt.% Ag composite materials.*

| Element Number | Element Symbol | Element Name | Atomic Conc. | Weight Conc. |
|---|---|---|---|---|
| 8 | O | Oxygen | 68.56 | 39.51 |
| 22 | Ti | Titanium | 28.80 | 49.65 |
| 47 | Ag | Silver | 2.38 | 9.26 |
| 83 | Bi | Bismuth | 0.19 | 1.42 |
| 29 | Cu | Copper | 0.07 | 0.16 |

A UV-visible light spectrum analyzer was used to analyze a mixture of 0.1 g of $CuBi_2O_4/TiO_2$ and $CuBi_2O_4/TiO_2$ powder doped with varying concentrations of Ag in 125 ml of a 10 ppm methylene blue dye solution. Methylene blue dye solvent samples were extracted and centrifuged every 20 minutes during the experiment; the methylene blue concentration was measured, and the samples' degradation of methylene blue was observed within 120 minutes. Fig. 8 (a)~(h) shows the results and spectra of the two-hour degradation experiment of eight samples in 125 ml of a solution initially containing 10 ppm of methylene blue. Fig. 9 shows the changes in the methylene blue solution containing $CuBi_2O_4/TiO_2$/11 wt.% Ag photocatalyst under UV light irradiation for two hours. The methylene blue solution was sampled at 20-minute intervals to measure its concentration. The color of the solution changes from blue to blue. Gradually, it turns to light blue. Fig. 10 shows a graph of the degradation rates of all samples. The degradation efficiency values are 48.37, 53.23, 59.48, 62.68, 69.60, 75.67, 82.65 and 78.43%, respectively. The results show that with the $CuBi_2O_4/TiO_2$/11 wt.% Ag photocatalyst, methylene blue degradation reaches the highest level, while with $CuBi_2O_4/TiO_2$/13 wt.% Ag, the degradation of methylene blue begins to reverse.

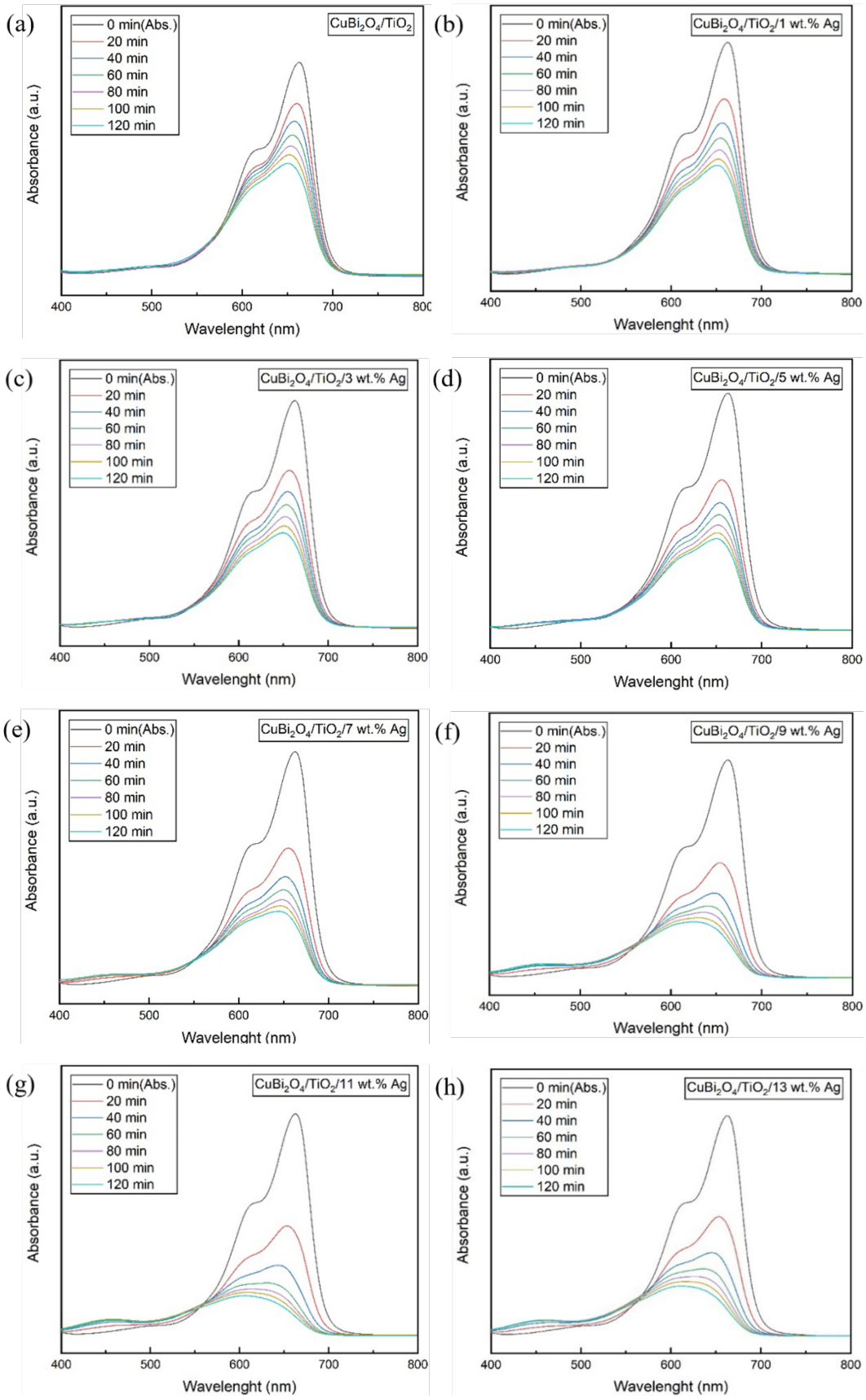


*Fig. 8. Absorption spectra for MB solution in the presence of (a) $CuBi_2O_4/TiO_2$ composite materials under UV-light irradiation and (b)~(h) with 1~13 wt.% Ag under UV-light irradiation.*

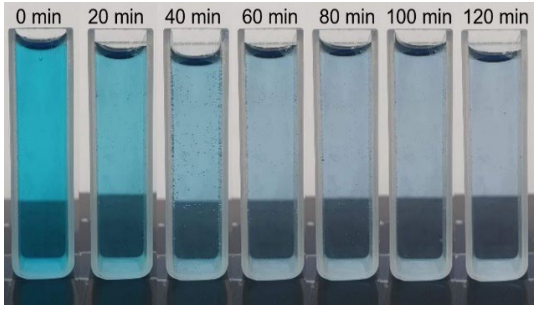


*Fig. 9. The degradation changes of the MB solution containing $CuBi_2O_4/TiO_2$/11 wt.% Ag photocatalyst under UV-light irradiation for 2 hours.*

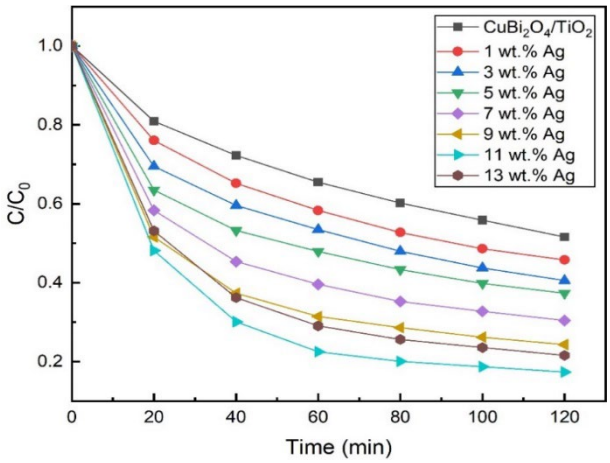


*Fig. 10. The concentration changes of MB solution in two hours in the presence of $CuBi_2O_4/TiO_2$/Ag composite materials under UV-light irradiation.*

In the UV-Vis absorption analysis, the light absorption properties of the prepared $CuBi_2O_4/TiO_2$ and $CuBi_2O_4/TiO_2$/Ag were evaluated by measuring the UV-Vis absorption spectra within the wavelength range of 300~800 nm. The results are shown in Fig. 11, which shows the absorption intensity of $CuBi_2O_4/TiO_2$ and $CuBi_2O_4/TiO_2$ powders doped with different concentrations of Ag. However, with Ag doping levels rising to 11%, the absorption intensity in the visible light region increases. However, with an increase in Ag content to 13%, there is a slight decrease in absorption within the visible range. This result shows that $CuBi_2O_4/TiO_2$/11 wt.% Ag has better absorption properties than base $CuBi_2O_4/TiO_2$.

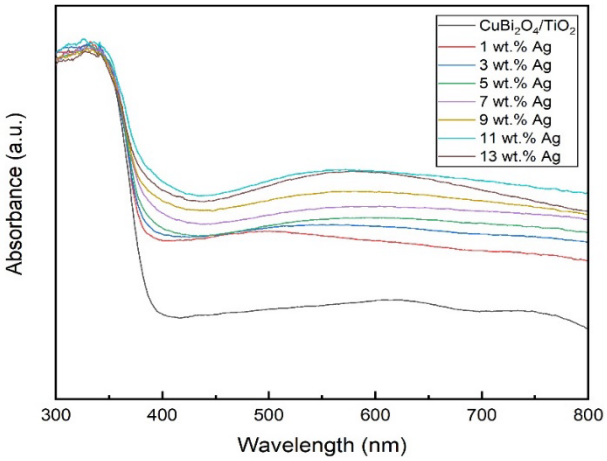


*Fig. 11. UV-vis absorption spectra of different $CuBi_2O_4/TiO_2$ doped with 1~13 wt.% Ag.*

The optical properties of $CuBi_2O_4/TiO_2$/Ag were detected through UV-visible light absorption spectroscopy [46] since $CuBi_2O_4$ and $TiO_2$ are direct band gap and indirect band gap materials respectively. The Kubelka-Munk function and the $(\alpha h\nu)^{1/n}$ versus h$\nu$ plot allow for the estimation of the band gap values of $CuBi_2O_4$, $CuBi_2O_4/TiO_2$, and $CuBi_2O_4/TiO_2$ with 11 wt.% Ag. For index n, the value is n=2 for indirect band gap semiconductors and n=0.5 for direct band gap semiconductors. The results are shown in Fig. 12 (a), (b), and (c). The corresponding band gaps of $CuBi_2O_4$, $CuBi_2O_4/TiO_2$, and $CuBi_2O_4/TiO_2$/11 wt.% Ag are estimated to be 1.49, 3.24, and 3.19 eV, respectively. The relationship between $(\alpha h\nu)^{1/n}$ and photon energy h$\nu$ according to equation (3) [34]:

$$(\alpha h\nu)^{1/n} = C(h\nu - Eg) \tag{3}$$

where $\alpha$ represents the absorption coefficient, $\nu$ represents the optical frequency, $Eg$ represents the band gap energy, and $C$ represents a constant [34, 47-49].

To investigate the optical properties of the prepared photocatalysts, UV-visible diffuse reflectance spectroscopy was employed. $CuBi_2O_4$ possesses a narrow bandgap of 1.5 eV and is designed to excite light under visible light. By contrast, $TiO_2$, with its wide band gap of around 3.2 eV, requires ultraviolet light for excitation. Thus, the conduction band (CB) and valence band (VB) of $CuBi_2O_4$ and $TiO_2$ can be determined using the following equations [34, 50]:

$$E_{VB} = X - E_e + 0.5E_g \tag{4}$$

$$E_{CB} = E_{VB} - E_g \tag{5}$$

In the formula, $E_{CB}$ and $E_{VB}$ correspond to the energy at the edge of the conduction band and valence band, respectively. *X* represents the absolute electronegativity of the semiconductor, which is the geometric average electronegativity of the atoms. The *X* values of $CuBi_2O_4$ and $TiO_2$ are 4.75 eV [51, 52] and 5.81 eV [51, 53], respectively; *Eg* represents the energy gap in a semiconductor, while *Ee* represents the free electron energy at the hydrogen potential (4.5 eV). Subsequently, the CB and VB values for $CuBi_2O_4$ were determined to be -0.5 eV and 1 eV, respectively, while for $TiO_2$, they were calculated as -0.29 eV and 2.91 eV, respectively.

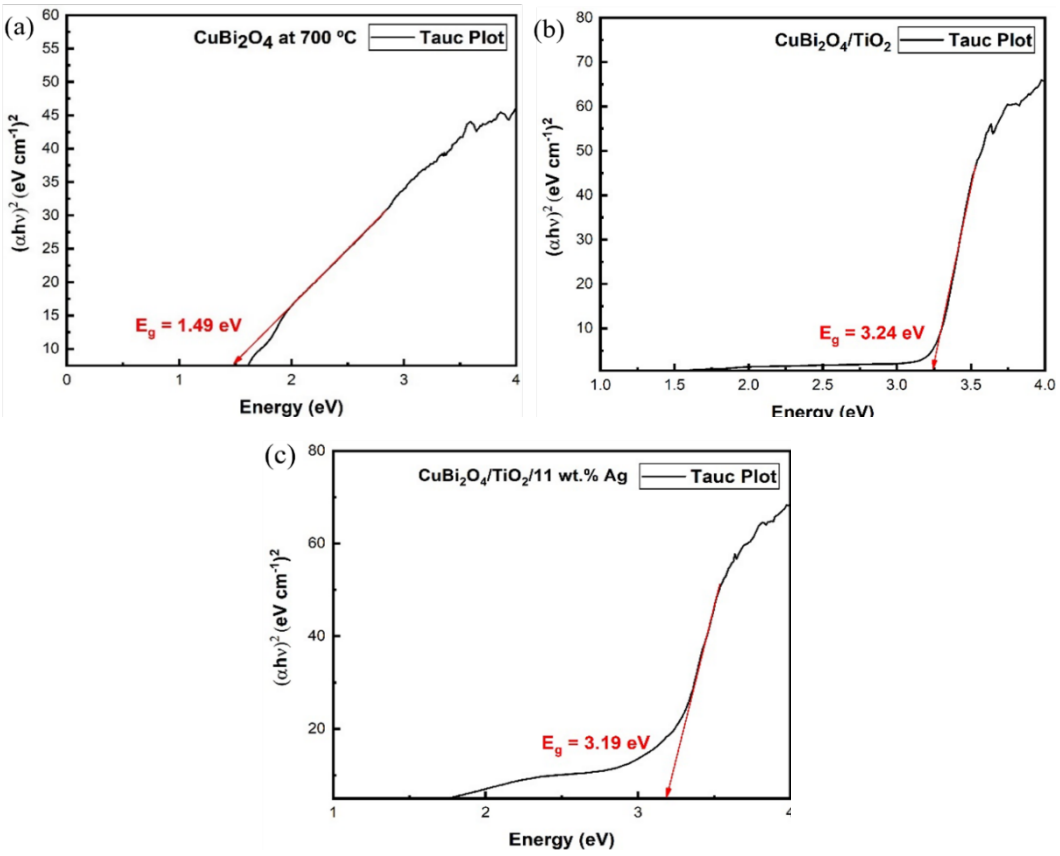


*Fig. 12. Bandgap of (a) $CuBi_2O_4$, (b) $CuBi_2O_4/TiO_2$, and (c) $CuBi_2O_4/TiO_2$/11 wt.% Ag.*

Fig. 13 illustrates a schematic representation of the potential mechanism for photocatalytic degradation of MB by $CuBi_2O_4/TiO_2$/Ag under UV light irradiation. Under UV light irradiation, for $CuBi_2O_4/TiO_2$ heterojunction photocatalyst and doped Ag, the electrons ($e^-$) on the VB of the $CuBi_2O_4$ catalyst are excited to the CB of the $TiO_2$ catalyst, so at the same time $CuBi_2O_4$ leaves a larger number of holes ($h^+$) on the VB. In addition, since the CB of $TiO_2$ is -0.29 eV and cannot reach the $O_2/•O^{2-}$ standard reduction potential (-0.33 eV) [54], the electrons ($e^-$) on $TiO_2$ conduction cannot reduce $O_2$ to $•O^{2-}$. Moreover, the holes in the valence band (1 eV) of $CuBi_2O_4$ are not enough to oxidize $OH^-/H_2O$ to •OH because of the standard oxidation potential of $OH^-$/•OH and $H_2O$/•OH

(+1.99 eV) [54, 56, 57]. Due to this specific bandgap situation, proposing a Z-scheme heterojunction is feasible. The photoexcited electrons ($e^-$) in the $TiO_2$ conduction band and the holes ($h^+$) in the $CuBi_2O_4$ valence band quickly combine under UV light irradiation. Excited electrons can be retained on the CB of $CuBi_2O_4$ due to their high electronegative nature and easy migration to the surface of $CuBi_2O_4$, and they can be reduced with $O_2$ to generate $\bullet O^{2-}$. Simultaneously, the large amount of $h^+$ released from the valence band of $TiO_2$ can successfully degrade contaminant MB into harmless products. This result demonstrates that the Z-type mechanism efficiently inhibits the recombination of photogenerated electron-hole pairs in semiconductor materials, thereby allowing the $CuBi_2O_4/TiO_2$ semiconductor material to exhibit excellent photocatalytic performance for MB degradation [54]. Furthermore, with the introduction of Ag into the $CuBi_2O_4/TiO_2$ system, the specific surface area increases, at least within a certain doping range [58, 59]. Although Ag lacks photocatalytic properties, its performance in photodegradation is subpar. [58, 59]. Introducing Ag into the $CuBi_2O_4/TiO_2$ coupling system results in a Schottky barrier at the silver-semiconductor interface, reducing the recombination of photogenerated electrons ($e^-$) and holes ($h^+$), thus extending their lifetimes [58, 60, 61]. This occurs because Ag has a lower Fermi level compared to $CuBi_2O_4$ and $TiO_2$, allowing it to act as an electron trap when present on the catalyst surface [58]. "Additionally, these electrons can enhance the rate of oxygen photoreduction and increase the quantity of photogenerated hydroxyl radicals [58, 62]. Furthermore, an excess of Ag on the catalyst surface forms a physical barrier to incident electromagnetic radiation, reflecting ultraviolet rays [58].

Among these prepared samples, the $CuBi_2O_4/TiO_2$/11 wt.% Ag composite photocatalyst exhibited the highest light harvesting. This is primarily due to the outstanding light absorption characteristics of the $CuBi_2O_4/TiO_2$ photocatalyst. As the amount of Ag doping increases, further improving the light-harvesting efficiency provides an opportunity to enhance ultraviolet light-induced photocatalysis.

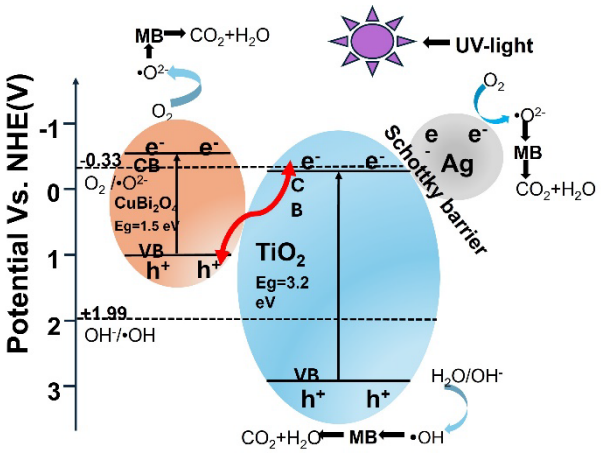


*Fig. 13. Schematic diagram of the possible mechanism of $CuBi_2O_4/TiO_2$/Ag degradation of methylene blue dye under UV light irradiation.*

Photoluminescence (PL) emission spectroscopy is extensively utilized to assess the efficiency of carrier capture, migration, and transfer. This technique is significantly related to understanding the electron-hole recombination rate in semiconductor particles [47]. Light electroluminescence emission is the result of free carrier recombination. An increase in PL intensity corresponds to a higher carrier recombination rate, whereas a decrease in PL intensity indicates a lower carrier recombination rate. Therefore, this study used 260 nm ultraviolet light as the excitation source. The photoluminescence emission spectra for $CuBi_2O_4/TiO_2$ and Ag-doped $CuBi_2O_4/TiO_2$ photocatalysts were detected over a wavelength range of 350 to 500 nm [3-6, 28], as shown in Fig. 14. The trend of the resulting PL spectrum shows that the PL emission intensity of $CuBi_2O_4/TiO_2$ with 11 wt.% Ag is considerably lower compared to the original $CuBi_2O_4/TiO_2$, which shows the photogenerated carrier recombination rate in $CuBi_2O_4/TiO_2$/11 wt.% Ag lowest, which also suggests that the photocathode exhibits lower PL intensity, resulting in a reduced photogenerated carrier recombination rate. Elevated Ag concentrations may function as recombination centers, promoting unwanted charge recombination and consequently diminishing the material's photocatalytic performance. The $CuBi_2O_4/TiO_2$/13 wt.% Ag photocathode exhibits greater PL intensity compared to the more efficient $CuBi_2O_4/TiO_2$/11 wt.% Ag photocathode, enhancing the recombination of photogenerated carriers.

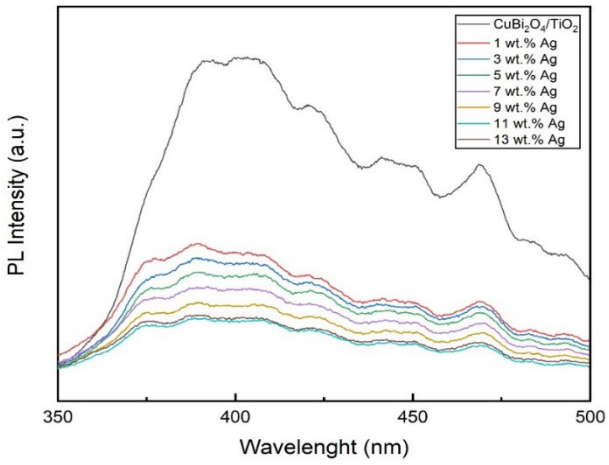


*Fig. 14. Photoluminescence spectra of different $CuBi_2O_4/TiO_2$ doped with 1~13 wt.% Ag.*

## 4. Conclusions

In this study, $CuBi_2O_4$ material was synthesized using the solid-state reaction method and subsequently combined with $TiO_2$ in varying proportions. The optimal ratio was 1:5. The degradation efficiency of the methylene blue dye solution dye reached 48.47%. In addition, different concentrations of Ag are doped to form heterostructure composites. The Ag-doped catalyst degrades

methylene blue when exposed to UV light. The $CuBi_2O_4/TiO_2$/11 wt.% Ag heterostructure nanocatalyst demonstrated superior photocatalytic activity, achieving a degradation efficiency of 82.65%, a significant improvement of 34.28% over the original 48.37% of $CuBi_2O_4/TiO_2$. A tetragonal geometric structure was observed in the XRD measurement, and $CuBi_2O_4$ was successfully synthesized at 700 °C. It was observed in the SEM images that, except for the unground $CuBi_2O_4$, there was no noticeable difference in the appearance morphology of the other eight sample powders, and their grain sizes ranged from 26 to 36 nm. Judging from the atomic distribution analyzed by EDS and mapping measurements, the powder is evenly mixed, and the atomic concentration and weight ratio of each element are similar. Finally, the photocatalytic mechanism of $CuBi_2O_4/TiO_2$ in the Ag-doped heterostructure nanocatalyst was discussed. Increasing the Ag content boosts the light-harvesting efficiency, thereby enhancing the UV-induced degradation capability of methylene blue dye.

## Acknowledgments

The authors acknowledge the support by the National Science and Technology Council, Taiwan, under grant number NSTC 113-2221-E-992-067-MY3 and Industry Cooperation Project no. 113A00262.

## References

[1] K. C. Hsu, T. H. Fang, C. I. Lee, T. H. Chen, T. H. Hsieh, Top. Catal. 63, 956-963 (2020); https://doi.org/10.1007/s11244-020-01300-4

[2] I. P. Tai, K. C. Hsu, I. T. Tang, T. H. Fang, T. C. Cheng, W. H. Wang, M. A. Ansari, C. J. Shih, Sens. Mater. 35(3), 1069-1080 (2023); https://doi.org/10.18494/SAM4233

[3] A. Bratovčić, Technological Acta 11(2), 17-23 (2019).

[4] M. Pirilä, M. Saouabe, S. Ojala, B. Rathnayake, F. Drault, A. Valtanen, M. Huuhtanen, R. Brahmi, R. L. Keiski, Top. Catal. 58, 1085 (2015); https://doi.org/10.1007/s11244-015-0477-7

[5] J. Luo, W. Chen, H. Song, J. Liu, Sci. Total Environ. 699, 134398 (2020); https://doi.org/10.1016/j.scitotenv.2019.134398

[6] S. Ahmed, M. G. Rasul, W. N. Martens, R. Brown, M. A. Hashib, Water Air Soil Pollut. 215, 3-29 (2011); https://doi.org/10.1007/s11270-010-0456-3

[7] W. J. Chen, K. C. Hsu, T. H. Fang, C. I. Lee, T. H. Chen, T. H. Hsieh, Dig. J. Nanometer. Bios. 16(4), 1227-1234 (2021).

[8] S. M. Al-Shomar, W. R. Alahmad, Dig. J. Nanometer. Bios. 14, 617 (2019).

[9] S. Sujinnapram, S. Nilphai, S. Moungsrijun, S. Krobthong, S. Wongrerkdee, Dig. J. Nanometer. Bios. 16, 317 (2021).

[10] B. P. Reddy, V. Rajendar, M. C. Shekar, S. H. Park, Dig. J. Nanometer. Bios. 13, 87 (2018).

[11] M. Javed, M. A. Abid, S. Hussain, D. Shahwar, S. Arshad, N. Ahmad, M. Arif, H. Khan, S. Nadeem, H. Raza, S. M. Harron, Dig. J. Nanometer. Bios. 15, 1097 (2020).

[12] C. Zörer, O. Baytar, Ö. Şahin, S. Horoz, M. S. Izgı, Dig. J. Nanometer. Bios. 15, 629 (2020).

[13] A. Modwi, B.R Y. Abdulkhair, M. E. Salih, N. Y. Elamin, A. M. Fatima, Dig. J. Nanometer. Bios. 14, 357 (2019).

[14] C. Xu, P. R. Anusuyadevi, C. Aymonier, R. Luque, S. Marre, Chem. Soc. Rev. 48, 3868 (2019); https://doi.org/10.1039/C9CS00102F

[15] Y. Sun, E. D. Liu, L. Zhu, Y. Wen, Q. W. Tan, W. Feng, Dig. J. Nanometer. Bios. 14, 463 (2019).

[16] Y. Sun, Q. Liu, L. Zhu, Q. W. Tan, Y. X. Fan, B. S. Zhao, J. Guo, Q. Q. Kong, Dig. J. Nanometer. Bios. 14, 139 (2019).

[17] S. M. Al-Shomar, W. R. Alahmad, Dig. J. Nanometer. Bios. 14, 617 (2019).

[18] S. Sujinnapram, S. Nilphai, S. Moungsrijun, S. Krobthong, S. Wongrerkdee, Dig. J. Nanometer. Bios. 16, 317 (2021).

[19] B. P. Reddy, V. Rajendar, M. C. Shekar, S. H. Park, Dig. J. Nanometer. Bios. 13, 87 (2018).

[20] M. Javed, M. A. Abid, S. Hussain, D. Shahwar, S. Arshad, N. Ahmad, M. Arif, H. Khan, S. Nadeem, H. Raza, S. M. Harron, Dig. J. Nanometer. Bios. 15, 1097 (2020).

[21] C. Zörer, O. Baytar, Ö. Şahin, S. Horoz, M. S. Izgi, Dig. J. Nanometer. Bios. 15, 629 (2020); https://doi.org/10.15251/DJNB.2020.153.629

[22] A. Modwi, B. R. Y. Abdulkhair, M. E. Salih, N. Y. Elamin, A. M. Fatima, Dig. J. Nanometer. Bios. 14, 357 (2019).

[23] Y. Sun, E. D. Liu, L. Zhu, Y. Wen, Q. W. Tan, W. Feng, Dig. J. Nanometer. Bios. 14, 463 (2019).

[24] Y. Sun, Q. Liu, L. Zhu, Q. W. Tan, Y. X. Fan, B. S. Zhao, J. Guo, Q. Q. Kong, Dig. J. Nanometer. Bios. 14, 139 (2019).

[25] E. Abdelkader, L. Nadjia, B. Ahmed, J. King Saud Univ. Sci. 27, 76-91 (2015); https://doi.org/10.1016/j.jksus.2014.06.002

[26] K. Zhang, F. J. Zhang, M. L. Chen, W. C. Oh, Ultrason. Sonochem. 18, 765-772 (2011); https://doi.org/10.1016/j.ultsonch.2010.11.008

[27] P. S. Basavarajappa, S. B. Patil, N. Ganganagappa, K. R. Reddy, A. V. Raghu, Ch. V. Reddy, Int. J. Hydrog. Energy 45, 7764 (2020); https://doi.org/10.1016/j.ijhydene.2019.07.241

[28] L. Wei, C. Shifu, Z. Sujuan, Z. Wei, Z. Huaye, Y. Xiaoling, J. Nanopart. Res. 12, 1355-1366 (2010); https://doi.org/10.1007/s11051-009-9672-4

[29] M. Ismael, Fuel 303, 121207 (2021); https://doi.org/10.1016/j.fuel.2021.121207

[30] C. B. Anucha, I. Altin, E. Bacaksiz, V. N. Stathopoulos, Chem. Eng. J. Adv. 10, 100262 (2022); https://doi.org/10.1016/j.ceja.2022.100262

[31] S. Kaur, V. Singh, J. Hazard. Mater. 141, 230-236 (2007); https://doi.org/10.1016/j.jhazmat.2006.06.123

[32] Q. Guo, C. Zhou, Z. Ma, X. Yang, Adv. Mater. 31, 1901997 (2019); https://doi.org/10.1002/adma.201901997

[33] C. H. Chiou, C. Y. Wu, R. S. Juang, Chem. Eng. J. 139, 322-329 (2008); https://doi.org/10.1016/j.cej.2007.08.002

[34] Y. Lu, K. Zhao, Y. Zhao, S. Zhu, X. Yuan, M. Huo, Y. Zhang, Y. Qiu, Colloid Surf. A-Physicochem. Eng. Asp. 481, 252-260 (2015); https://doi.org/10.1016/j.colsurfa.2015.05.037

[35] N. Ghows, M. H. Entezari, J. Hazard. Mater. 195, 132-138 (2011); https://doi.org/10.1016/j.jhazmat.2011.08.049

[36] F. Zhang, Y. Sun, M. Li, Q. Wang, W. Song, J. Ma, J. Hou, Colloid Surf. A-Physicochem. Eng. Asp. 667, 131389 (2023); https://doi.org/10.1016/j.colsurfa.2023.131389

[37] H. Ramezanalizadeh, E. Rafiee, Mater. Sci. Semicond. Process 113, 105055 (2020); https://doi.org/10.1016/j.mssp.2020.105055

[38] A. Song, P. Bogdanoff, A. Esau, I. Y. Ahmet, I. Levine, T. Dittrich, T. Unold, R. V. D. Krol, S. P. Berglund, ACS Appl. Mater. Interfaces 12, 13959-13970 (2020); https://doi.org/10.1021/acsami.0c00696

[39] W.i Lu, T. T. Gu, X. Jing, Y. Zhu, L. Yu, S. Hou, T. Pang, N. Lu, Z. Zhang, J. Alloy. Compd. 968, 171864 (2023); https://doi.org/10.1016/j.jallcom.2023.171864

[40] H. Zhou, J. Pan, L. Ding, Y. Tang, J. Ding, Q. Guo, T. Fan, D. Zhang, Int. J. Hydrog. Energy 39, 16293 (2014); https://doi.org/10.1016/j.ijhydene.2014.08.032

[41] C. Moslah, M. Kandyla, G. A. Mousdis, G. Petropoulou, M. Ksibi, Phys. Status Solidi A-Appl. Mat. 215, 1800023 (2018); https://doi.org/10.1002/pssa.201800023

[42] H. H. Mohamed, D. W. Bahnemann: Appl. Cartel. B 128, 91 (2012); https://doi.org/10.1016/j.apcatb.2012.05.045

[43] Y. Liu, Q. Zhang, M. Xu, H. Yuan, Y. Chen, J. Zhang, K. Luo, J. Zhung, B. You: Appl. Surf. Sci. 476, 632 (2019); https://doi.org/10.1016/j.apsusc.2019.01.137

[44] N. Ahmad, J. Anae, M. Z. Khan, S. Sabir, P. Campo, F. Coulon, Heliyon 8, e10210 (2022); https://doi.org/10.1016/j.heliyon.2022.e10210

[45] G. Sharma, Z. Zhao, P. Sarker, B. A. Nail, J. Wang, M. N. Huda, F. E. Osterloh, J. Mater. Chem. A 4, 2936-2942 (2016); https://doi.org/10.1039/C5TA07040F

[46] H. Cao, H. Yu, Y. Lu, H. Zhang, G. Hou, Y. Tang, G. Zheng, ChemistrySelect 5, 5137-5145 (2020); https://doi.org/10.1002/slct.202000557

[47] K. Liu, N. Li, J. Ding, N. Chen, S. Wang, Q. Wang, X. Yao, X. Li, J. Wang, H. Yin, Chemosphere 324, 138357 (2023); https://doi.org/10.1016/j.chemosphere.2023.138357

[48] X. Zhang, S. Wang, C. Pan, Y. Zeng, Mater. Lett. 288, 129388 (2021); https://doi.org/10.1016/j.matlet.2021.129388

[49] T. Saison, N. Chemin, C. Chaneac, O. Durupthy, V. Ruaux, L. Mariey, F. Mauge, P. Beaunier, J. P. Jolivet, J. Phys. Chem. C 115, 5657-5666 (2011); https://doi.org/10.1021/jp109134z

[50] P. Ju, P. Wang, B. Li, H. Fan, S. Y. Ai, D. Zhang, Y. Wang, Chem. Eng. J. 236, 430-437 (2014); https://doi.org/10.1016/j.cej.2013.10.001

[51] A. S. Mary, C. Murugan, A. Pandikumar, J. Colloid Interface Sci. 608, 2482-2492 (2022); https://doi.org/10.1016/j.jcis.2021.10.172

[52] A. Elaziouti, N. Laouedj, A. Bekka, R. N. Vannier, J. King Saud Univ. Sci. 27, 120-135 (2015); https://doi.org/10.1016/j.jksus.2014.08.002

[53] X. Lu, Z. Liu, Dalton Trans. 46(30), 9886-9894 (2017); https://doi.org/10.1039/C7DT02214J

[54] X. Zhang, S. Wang, L. Lin, X. Tan, Y. Zeng, Colloid Surf. A-Physicochem. Eng. Asp. 614, 126008 (2021); https://doi.org/10.1016/j.colsurfa.2020.126008

[55] F. Guo, W. Shi, H. Wang, M. Han, W. Guan, H. Huang, Y. Liu, Z. Kang, J. Hazard. Mater. 349, 111-118 (2018); https://doi.org/10.1016/j.jhazmat.2018.01.042

[56] X. C. Meng, Z. S. Zhang, J. Photochem. Photobiol. A-Chem. 310, 33-44 (2015).

[57] Y. Liu, A. L. Yuan, Y. F. Xiao, H. J. Yu, X. P. Dong, Ceram. Int. 46, 16157-16165 (2020); https://doi.org/10.1016/j.ceramint.2020.03.171

[58] M. Pérez-González, S. A. Tomás, Catal. Today 360, 129-137 (2021); https://doi.org/10.1016/j.cattod.2019.08.009

[59] M. Pérez-González, S. A. Tomás, J. Santoyo-Salazar, S. Gallardo-Hernández, M. M. Tellez-Cruz, O. Solorza-Feria, J. Alloy. Compd. 779, 908-917 (2019); https://doi.org/10.1016/j.jallcom.2018.11.302

[60] J. Tao, Z. Gong, G. Yao, Y. Cheng, M. Zhang, J. Lv, S. Shi, G. He, X. Jiang, X. Chen, Z. Sun, J. Alloy. Compd. 688, 605-612 (2016); https://doi.org/10.1016/j.jallcom.2016.07.074

[61] S. A. Tomás, A. Luna-Resendis, L. C. Cortés-Cuautli, D. Jacinto, Thin Solid Films 518, 1337-1340 (2009); https://doi.org/10.1016/j.tsf.2009.03.219

[62] M. R. Espino-Estévez, C. Fernández-Rodríguez, O. M. González-Díaz, J. Araña, J. P. Espinós, J. A. Ortega-Méndez, J. M. Doña-Rodríguez, Chem. Eng. J. 298, 82-95 (2016); https://doi.org/10.1016/j.cej.2016.04.016